PHYSICAL REVIEW D **90,** 016007 (2014)

Unifying "soft" and "hard" diffractive exclusive vector meson production and deeply virtual Compton scattering

S. Fazio,[1,*] R. Fiore,[2,†] L. Jenkovszky,[3,‡] and A. Salii[3,§]

[1]*Brookhaven National Laboratory, Physics Department, 11973 Upton, New York, USA*
[2]*Dipartimento di Fisica, Universitá della Calabria and Istituto Nazionale di Fisica Nucleare, Gruppo collegato di Cosenza I-87036 Arcavacata di Rende, Cosenza, Italy*
[3]*Bogolyubov Institute for Theoretical Physics National Academy of Sciences of Ukraine, UA-03680 Kiev, Ukraine*

(Received 11 February 2014; published 10 July 2014)

A Pomeron model applicable to both "soft" and "hard" processes is suggested and tested against the high-energy data from virtual photon-induced reactions. The Pomeron is universal, containing two terms, a soft and a hard one, whose relative weight varies with $\widetilde{Q^2} = Q^2 + M_V^2$, where Q^2 is the virtuality of the incoming photon and M_V is the mass of the produced vector particle. With a small number of adjustable parameters, the model fits all available data on vector meson production and deeply virtual Compton scattering from HERA. Furthermore, we attempt to apply the model to hadron-induced reactions, by using high-energy data on proton-proton scattering.

DOI: 10.1103/PhysRevD.90.016007 PACS numbers: 11.55.Jy, 12.40.Nn, 13.60.Le, 13.60.Fz

I. INTRODUCTION

According to perturbative QCD calculations, the Pomeron corresponds to the exchange of an infinite gluon ladder, producing an infinite set of moving Regge poles, the so-called BFKL Pomeron [1], whose highest intercept $\alpha(0)$ is near $1.3 \div 1.4$. Phenomenologically, "soft" (low virtuality Q^2) and "hard" (high virtuality Q^2) diffractive (i.e. small squared momentum transfer t) processes with Pomeron exchange are described by the exchange of two different objects in the t channel, a "soft" and a "hard" Pomeron (or their QCD images, see, for instance, Refs. [2,3]). This implies the existence of two (or even more) scattering amplitudes, differing by the values of the parameters of the Pomeron trajectory, their intercept $\alpha(0)$ and slope $\alpha'(t=0)$, typically $(1.08 \div 1.09)$ and (0.25), respectively, for the "soft" Pomeron, and $(1.3 \div 1.4)$ and (0.1 or even less) for the "hard" one, each attached to vertices of the relevant reaction or kinematical region. A simple "unification" consists in making these parameters Q^2-dependant, although this breaks Regge factorization, by which Regge trajectories should not depend on Q^2.

In the present approach, initiated in Refs. [4,5], we postulate that:

(i) Regge factorization holds, i.e., the dependence on the virtuality of the external particle (virtual photon) enters only the relevant vertex, not the propagator;
(ii) there is only one Pomeron in nature and it is the same in all reactions. It may be complicated, e.g. having many, at least two, components.

The first postulate was applied, for example, in Refs. [5–7] to study deeply virtual Compton scattering (DVCS) and vector meson production (VMP). In Fig. 1, where diagrams (a) and (b) represent the DVCS and the VMP, respectively, the Q^2 dependence enters only the upper vertex of the diagram (c). The particular form of this dependence and its interplay with t is not unique.

In Refs. [5,7] the interplay between t and Q^2 was realized by the introduction of a new variable, $z = t - \widetilde{Q^2}$, where $\widetilde{Q^2}$ is the familiar variable $\widetilde{Q^2} = Q^2 + M_V^2$, here M_V is a vector meson mass. The model (called also "scaling model") is simple and fits the data on DVCS (with $M_V = 0$) and VMP, although the physical meaning of this new variable is not clear.

In a series of subsequent papers (see Refs. [4,7,8]), $\widetilde{Q^2}$ was incorporated in a "geometrical" way reflecting the observed trend in the decrease of the forward slope as a function of $\widetilde{Q^2}$. This geometrical approach, combined with the Regge-pole model was named "Reggeometry". A Reggeometric amplitude dominated by a single Pomeron shows [4] reasonable agreement with the HERA data on VMP and DVCS, when fitted separately to each reaction, i.e., with a large number of parameters adjusted to each particular reaction.

As a further step, to reproduce the observed trend of hardening as $\widetilde{Q^2}$ increases,[1] and following Donnachie and Landshoff [9,10], a two-term amplitude, characterized by a two-component - "soft" + "hard" - Pomeron, was suggested [4]. We stress that the Pomeron is unique, but we

*sfazio@bnl.gov
†roberto.fiore@cs.infn.it
‡jenk@bitp.kiev.ua
§saliy.andriy@gmail.com

[1]In what follows we use the variable $\widetilde{Q^2}$ as a measure of "hardness."

 © 2014 American Physical Society

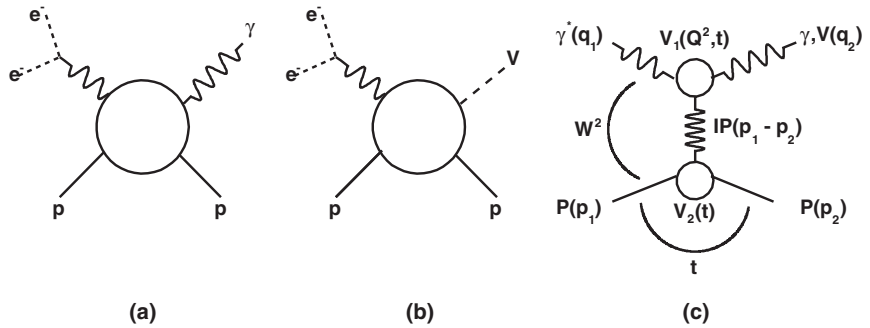

FIG. 1. Diagrams of DVCS (a) and VMP (b); (c) DVCS (VMP) amplitude in a Regge-factorized form.

construct it as a sum of two terms. Then, the amplitude is defined as

$$A(\widetilde{Q^2},s,t)=A_s(\widetilde{Q^2},s,t)+A_h(\widetilde{Q^2},s,t), \tag{1}$$

($s=W^2$ is the square of the c.m.s. energy), such that the relative weight of the two terms changes with $\widetilde{Q^2}$ in a right way (see Fig. 14), i.e. such that the ratio $r=A_h/A_s$ increases as the reaction becomes "harder" and v.v. It is interesting to note that this trend is not guaranteed "automatically," and it should be defined "by hand." In [9,10] it was corrected by means of additional $\widetilde{Q^2}$-dependent factors $H_i(\widetilde{Q^2}), i=s,h$ modifying the $\widetilde{Q^2}$ dependence of the amplitude, in a such way as to provide increasing of the weight of the hard component with increasing $\widetilde{Q^2}$. To avoid conflict with unitarity, the rise with $\widetilde{Q^2}$ of the hard component is finite (or moderate), and it terminates at some saturation scale, whose value is determined phenomenologically. In other words, the "hard" component, invisible at small $\widetilde{Q^2}$, gradually takes over the soft one as $\widetilde{Q^2}$ increases. An explicit example of these functions will be given below.

This paper is organized as follows. In Sec. II we recall and update the single-component Reggeometric model of Ref. [4]. In Sec. III the model is extended to a two-component Pomeron: "soft" + "hard." A global fit to the HERA data on all VMP and DVCS, with a unique (and small) number of parameters, is presented. In Sec. IV the Q^2-dependent balance between the two components is studied. In Sec. V we attempt to unify virtual photon- and hadron-induced reactions taking high-energy pp scattering as an example. Hadron-hadron elastic scattering is different from exclusive VMP and DVCS not only because the photon is different from a hadron (although they are related by vector meson dominance), but even more so by the transition between space- and timelike regions: while the virtual photon's "mass square" q^2 is negative, that of the hadron is positive and that makes this attempt interesting. Our main results and the open questions are summarized in Sec. VI.

II. SINGLE-COMPONENT REGGEOMETRIC POMERON

We start by recalling the properties and some representative results of the single-term Reggeometric model [4].

The invariant scattering amplitude is defined as

$$A(Q^2,s,t)=\tilde{H}e^{-\frac{i\pi\alpha(t)}{2}}\left(\frac{s}{s_0}\right)^{\alpha(t)}e^{2\left(\frac{a}{\widetilde{Q^2}}+\frac{b}{2m_p^2}\right)t}, \tag{2}$$

where

$$\alpha(t)=\alpha_0+\alpha' t \tag{3}$$

is the linear Pomeron trajectory, s_0 is a scale for the square of the total energy s, a and b are two parameters to be determined with the fitting procedure and m_p is the proton mass. The coefficient $\tilde{H}$ is a function providing the right behavior of elastic cross sections in $\widetilde{Q^2}$:

$$\tilde{H}\equiv\tilde{H}(\widetilde{Q^2})=\frac{\tilde{A}_0}{\left(1+\frac{\widetilde{Q^2}}{Q_0^2}\right)^{n_s}}, \tag{4}$$

where $\tilde{A}_0$ is a normalization factor, Q_0^2 is a scale for the virtuality and n_s is a real positive number.

In this model one uses an effective Pomeron, which can be soft or hard, depending on the reaction and/or kinematical region defining its hardness. In other words, the values of the parameters α_0 and α' must be fitted to each set of the data. Apart from α_0 and α', the model contains five more sets of free parameters, different in each reaction, as shown in Table I. The exponent in the exponential factor in Eq. (2) reflects the geometrical nature of the model: $a/\widetilde{Q^2}$ and $b/2m_p^2$ correspond to the "sizes" of upper and lower vertices in Fig. 1c.

By using Eq. (4) with norm

$$\frac{d\sigma_{\rm el}}{dt}=\frac{\pi}{s^2}|A(Q^2,s,t)|^2, \tag{5}$$

the differential and integrated elastic cross sections become,

TABLE I. Values of the parameters in Eqs. (6), (7) fitted to data on VMP and DVCS at HERA. The parameters with unspecified error bars were fixed at the fitting stage.

Particle	$A_0\ (\frac{\sqrt{\text{nb}}}{\text{GeV}})$	$Q_0^2\ (\text{GeV}^2)$	n	α_0	$\alpha'\ (\frac{1}{\text{GeV}^2})$	a	b	$\tilde{\chi}^2$
pp	5.9 ± 3.3	$***$	0.00	1.05 ± 0.08	0.28 ± 0.28	2.9 ± 1.6	0.00	1.53
ρ^0	344 ± 376	0.29 ± 0.14	1.24 ± 0.07	1.16 ± 0.14	0.21 ± 0.53	0.60 ± 0.33	0.9 ± 4.3	2.74
ϕ	58 ± 112	0.89 ± 1.40	1.30 ± 0.28	1.14 ± 0.19	0.17 ± 0.78	0.0 ± 19.8	1.34 ± 5.09	1.22
J/ψ	30 ± 31	2.3 ± 2.2	1.45 ± 0.32	1.21 ± 0.09	0.077 ± 0.072	1.72	1.16	0.27
$\Upsilon(1S)$	37 ± 100	0.93 ± 1.75	1.45 ± 0.53	1.29 ± 0.25	0.006 ± 0.6	1.90	1.03	0.4
$DVCS$	14.5 ± 41.3	0.28 ± 0.98	0.90 ± 0.18	1.23 ± 0.14	0.04 ± 0.71	1.6	1.9 ± 2.5	1.05

$$\frac{d\sigma_{\text{el}}}{dt} = \frac{A_0^2}{\left(1+\frac{\widetilde{Q}^2}{Q_0^2}\right)^{2n}} \left(\frac{s}{s_0}\right)^{2(\alpha(t)-1)} e^{4\left(\frac{a}{\widetilde{Q}^2}+\frac{b}{2m_p^2}\right)t}, \tag{6}$$

and

$$\sigma_{\text{el}} = \frac{A_0^2}{\left(1+\frac{\widetilde{Q}^2}{Q_0^2}\right)^{2n}} \frac{\left(\frac{s}{s_0}\right)^{2(\alpha_0-1)}}{4\left(\frac{a}{\widetilde{Q}^2}+\frac{b}{2m_p^2}\right)+2\alpha' \ln\left(\frac{s}{s_0}\right)}, \tag{7}$$

where $A_0 = -(\sqrt{\pi}/s_0)\widetilde{A_0}$. For simplicity we set $s_0 = 1\ \text{GeV}^2$.

Equations (6) and (7) were fitted to the HERA data obtained by the ZEUS and H1 Collaborations on exclusive diffractive VMP [11–39] and DVCS [40–44].

In the present paper we have updated and extended the fits shown earlier in Ref. [4], the results being collected in Table I, where the parameters with unspecified error bars were fixed at the fitting stage. The "mass parameter" for DVCS was set $M = 0$ GeV, therefore in this case $\widetilde{Q^2} = Q^2$. Each type of reaction was fitted separately. Representative fits are shown in Fig. 2. The single-term model fails to fit both the high- and low-$|t|$ regions of light vector mesons low Q^2 production (photoproduction) properly. The reason of difficulty is that t also defines the softness of the process, thus low Q^2 light vector meson production comprises both soft and hard processes. The other problem of the single-term Reggeometric Pomeron model, Eq. (2), is that the fitted parameters in this model acquire particular values for each reaction, which is one of the motivations for its extension to two terms (see next section).

The VMP results clearly show the hardening of Pomeron in the change of α_0 and α' when going from light to heavy vector mesons. To describe production of all vector mesons at different (both soft and hard) regimes we introduce a two-component Pomeron model.

It is also interesting to note that the effective Pomeron trajectory for DVCS ($\alpha_0 = 1.23$, $\alpha' = 0.04$, see Table I) is typically a hard one, in contradiction to expectations, that it should be soft at low-Q^2.

III. TWO-COMPONENT REGGEOMETRIC POMERON

A. Amplitude with two, soft and hard, components

Now we introduce the universal, soft and hard, Pomeron model. Using the Reggeometric ansatz of Eq. (2), we write the amplitude as a sum of two parts, corresponding to the soft and hard components of a universal, unique Pomeron:

$$A(\widetilde{Q^2}, s, t) = \widetilde{H_s} e^{-i\frac{\pi}{2}\alpha_s(t)} \left(\frac{s}{s_{0s}}\right)^{\alpha_s(t)} e^{2\left(\frac{a_s}{\widetilde{Q^2}}+\frac{b_s}{2m_p^2}\right)t} + \widetilde{H_h} e^{-i\frac{\pi}{2}\alpha_h(t)} \left(\frac{s}{s_{0h}}\right)^{\alpha_h(t)} e^{2\left(\frac{a_h}{\widetilde{Q^2}}+\frac{b_h}{2m_p^2}\right)t}. \tag{8}$$

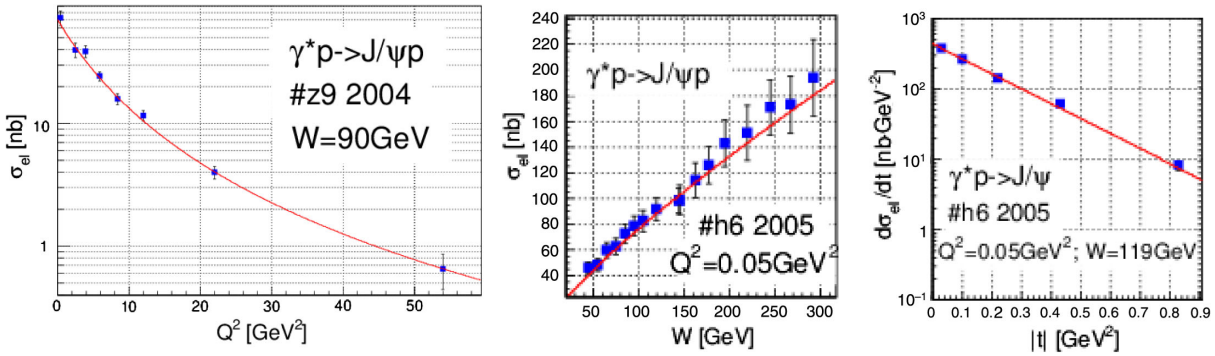

FIG. 2 (color online). Representative fits of Eqs. (6) and (7) to the data on J/ψ production. The values of the fitted parameters are compiled in Table I.

Here s_{0s} and s_{0h} are squared energy scales, and a_i and b_i, with $i = s, h$, are parameters to be determined with the fitting procedure. The two coefficients $\widetilde{H_s}$ and $\widetilde{H_h}$ are functions similar to those defined in Ref. [10]:

$$\widetilde{H_s} \equiv \widetilde{H_s}(\widetilde{Q^2}) = \frac{\widetilde{A_s}}{\left(1+\frac{\widetilde{Q^2}}{Q_s^2}\right)^{n_s}},$$
$$\widetilde{H_h} \equiv \widetilde{H_h}(\widetilde{Q^2}) = \frac{\widetilde{A_h}\left(\frac{\widetilde{Q^2}}{Q_h^2}\right)}{\left(1+\frac{\widetilde{Q^2}}{Q_h^2}\right)^{n_h+1}}, \tag{9}$$

where $\widetilde{A_s}$ and $\widetilde{A_h}$ are normalization factors, Q_s^2 and Q_h^2 are scales for the virtuality, n_s and n_h are real positive numbers. Each component of Eq. (8) has its own, soft or hard, Regge (here Pomeron) trajectory:

$$\alpha_s(t) = \alpha_{0s} + \alpha_s' t, \qquad \alpha_h(t) = \alpha_{0h} + \alpha_h' t.$$

As an input we use the parameters suggested by Donnachie and Landshoff [45], so that

$$\alpha_s(t) = 1.08 + 0.25t, \qquad \alpha_h(t) = 1.40 + 0.1t.$$

The "Pomeron" amplitude (8) is unique, valid for all diffractive reactions, its softness or hardness depending on the relative $\widetilde{Q^2}$-dependent weight of the two components, governed by the relevant factors $\widetilde{H_s}(\widetilde{Q^2})$ and $\widetilde{H_h}(\widetilde{Q^2})$.

Fitting Eq. (8) to the data, we have found that the parameters assume rather large errors and, in particular, the parameters $a_{s,h}$ are close to 0. Thus, in order to reduce the number of free parameters, we simplified the model, by fixing $a_{s,h} = 0$ and substituting the exponent $2(\frac{a_{s,h}}{\widetilde{Q^2}} + \frac{b_{s,h}}{2m_p^2})$ with $b_{s,h}$ in Eq. (8). The proper variation with $\widetilde{Q^2}$ will be provided by the factors $\widetilde{H_s}(\widetilde{Q^2})$ and $\widetilde{H_h}(\widetilde{Q^2})$.

Consequently, the scattering amplitude assumes the form

$$A(s,t,Q^2,M_V^2) = \widetilde{H_s}(\widetilde{Q^2}) e^{-i\frac{\pi}{2}\alpha_s(t)} \left(\frac{s}{s_{0s}}\right)^{\alpha_s(t)} e^{b_s t} + \widetilde{H_h}(\widetilde{Q^2}) e^{-i\frac{\pi}{2}\alpha_h(t)} \left(\frac{s}{s_{0h}}\right)^{\alpha_h(t)} e^{b_h t}. \tag{10}$$

The "Reggeometric" combination $2\left(\frac{a_{s,h}}{\widetilde{Q^2}} + \frac{b_{s,h}}{2m_p^2}\right)$ was important for the description of the slope $B(Q^2)$ within the single-term Pomeron model (see previous section), but in the case of two terms the Q^2-dependence of B can be reproduced without this extra combination, since each term in the amplitude (10) has its own Q^2-dependent factor $\widetilde{H_{s,h}}(Q^2)$.

By using the amplitude (10) and Eq. (5), we calculate the differential and elastic cross sections, by setting for simplicity $s_{0s} = s_{0h} = s_0$, to obtain

$$\frac{d\sigma_{\rm el}}{dt} = H_s^2 e^{2\{L(\alpha_s(t)-1)+b_s t\}} + H_h^2 e^{2\{L(\alpha_h(t)-1)+b_h t\}} + 2H_s H_h e^{\{L(\alpha_s(t)-1)+L(\alpha_h(t)-1)+(b_s+b_h)t\}} \times \cos\left(\frac{\pi}{2}(\alpha_s(t)-\alpha_h(t))\right), \tag{11}$$

$$\sigma_{\rm el} = \frac{H_s^2 e^{2\{L(\alpha_{0s}-1)\}}}{2(\alpha_s' L + b_s)} + \frac{H_h^2 e^{2\{L(\alpha_{0h}-1)\}}}{2(\alpha_h' L + b_h)} + 2H_s H_h e^{L(\alpha_{0s}-1)+L(\alpha_{0h}-1)} \frac{\mathfrak{B}\cos\phi_0 + \mathfrak{A}\sin\phi_0}{\mathfrak{B}^2+\mathfrak{A}^2}. \tag{12}$$

In these two equations we used the notations

$$L = \ln(s/s_0), \qquad \mathfrak{B} = L\alpha_s' + L\alpha_h' + (b_s + b_h),$$
$$\phi_0 = \frac{\pi}{2}(\alpha_{0s} - \alpha_{0h}), \qquad \mathfrak{A} = \tfrac{\pi}{2}(\alpha_s' - \alpha_h'),$$
$$H_s(\widetilde{Q^2}) = \frac{A_s}{\left(1+\frac{\widetilde{Q^2}}{Q_s^2}\right)^{n_s}}, \qquad H_h(\widetilde{Q^2}) = \frac{A_h\left(\frac{\widetilde{Q^2}}{Q_h^2}\right)}{\left(1+\frac{\widetilde{Q^2}}{Q_h^2}\right)^{n_h+1}},$$

with

$$A_{s,h} = -\frac{\sqrt{\pi}}{s_0}\widetilde{A_{s,h}}.$$

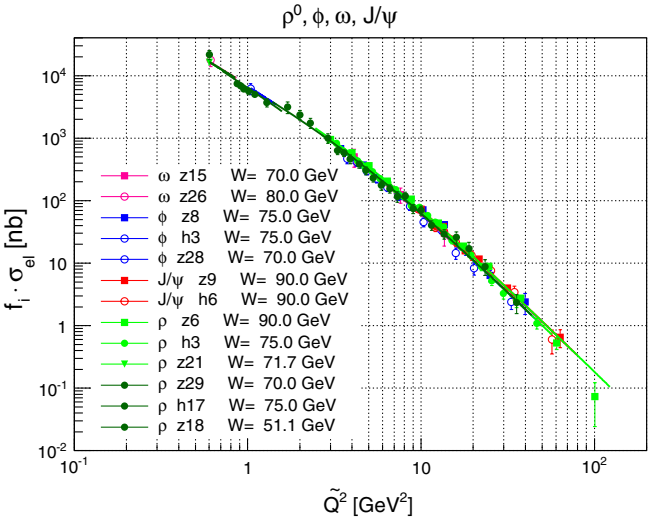

FIG. 3 (color online). Fit of Eq. (12) to the data on the normalized elastic cross section $f_i \cdot \sigma_{\rm el}(Q^2)$ for ρ^0, ϕ, ω and J/ψ, for different values of W. Here f_i is the normalization factor [see Eq. (15)].

TABLE II. Experimental data used.

Index	Cite	Year	Particle	W (GeV)	$< W >$	Q^2 (GeV^2)	$< Q^2 >$	$\lvert t\rvert$ (GeV^2)	Reaction type[a]	Luminosity (pb^{-1})	Data taking period	Decay mode
z1	[11]	2011	$\Upsilon(1S)$	60 ÷ 220	90	< 1	10^{-3}	< 5	php	468	[96 – 07]	$\mu^+\mu^-$
z4	[12]	2009	$\Upsilon(1S)$	60 ÷ 220		< 1	10^{-3}		php	468	[96 – 07]	$\mu^+\mu^-$
z19	[13]	1998	$\Upsilon(1S)$	80 ÷ 160	120	< 1	5×10^{-5}		php	43.2	[95 – 97]	$\mu^+\mu^-$
h15	[14]	2000	$\Upsilon(1S)$	70 ÷ 250	160	< 1	0.011	< 1.2	php	27.5	[94 – 97]	$\mu^+\mu^-$
			J/ψ	26 ÷ 285	160		0.05	< 1.2	php	20.5	[96 – 97]	$\mu^+\mu^-$, e^+e^-
h9	[15]	2002	$\psi(2s)$, J/ψ	40 ÷ 150		< 1	0.055	< 1.0	php	77	[96 – 00]	$\mu^+\mu^-$, e^+e^-, $J/\psi + \pi^+\pi^-$
h6	[16]	2005	J/ψ	40 ÷ 305	90	< 1	0.05	< 1.2	php	55	[99 – 00]	e^+e^-, $\mu^+\mu^-$
			J/ψ	40 ÷ 160	90	2 ÷ 80	8.9	< 1.2		55	[99 – 00]	
z9	[17]	2004	J/ψ	30 ÷ 220	90	.15 ÷ .8		< 1		69	[98 – 00]	e^+e^-
						2 ÷ 100				83		$\mu^+\mu^-$, e^+e^-
z13	[18]	2002	J/ψ	20 ÷ 290		< 1	5×10^{-5}	< 1.25	php	55.2	[99 – 00]	e^+e^-
				20 ÷ 170				< 1.8	php	38	[96 – 97]	$\mu^+\mu^-$
h16	[19]	1999	J/ψ	25 ÷ 180	96	2 ÷ 80	8	< 1.5		27.3	[95 – 97]	$\mu^+\mu^-$, e^+e^-
z24	[20]	1997	J/ψ	40 ÷ 140		< 4	5×10^{-3}	< 1	php	2.7	[94]	e^+e^-
										1.87		$\mu^+\mu^-$
z16	[21]	2000	J/ψ, ϕ, ρ	85 ÷ 105	94	< 0.01	7×10^{-6}	< 3	php	1.98	[95]	$J/\psi \to \mu^+\mu^-(e^+e^-)$, $\rho \to \pi^+\pi^-$, $\phi \to K^+K^-$
h3	[22]	2010	ϕ, ρ	35 ÷ 180		2.5 ÷ 60		< 3		51	[96 – 00]	$\rho \to \pi^+\pi^-$, $\phi \to K^+K^-$
z15	[23]	2000	ω, ϕ	40 ÷ 120	70	3 ÷ 20	7	< 0.6		37.7	[96 – 97]	$\pi^+\pi^-\pi^0$, $\pi^0 \to \gamma\gamma$
z26	[24]	1999	ω	70 ÷ 90	80	< 4	10^{-4}	< 0.6	php	3.2	[94]	$\pi^+\pi^-\pi^0$, $\pi^0 \to \gamma\gamma$
z8	[25]	2005	ϕ	35 ÷ 145	75	2 ÷ 70	5	< 0.6		65.1	[98 – 00]	K^+K^-
h14	[26]	2000	ϕ	40 ÷ 130	75	1 ÷ 5		< 0.5		0.125	[95]	K^+K^-
						2.5 ÷ 15				3	[96]	K^+K^-
h19	[27]	1997	ϕ	42 ÷ 134	100	6 ÷ 20		< 0.6		2.8	[94]	K^+K^-
z28	[28]	1996	ϕ	60 ÷ 80	70	< 4	10^{-1}	0.1 ÷ 0.5	php	0.887[b]	[94]	K^+K^-
z27	[29]	1996	ϕ	42 ÷ 134	98	7 ÷ 25	12.3	< 0.6		2.62	[94]	K^+K^-
z18	[30]	1998	J/ψ	50 ÷ 150	97	2 ÷ 40	5.9	< 1		6.0	[95]	e^+e^-, $\mu^+\mu^-$
			ρ	20 ÷ 90	47	.25 ÷ .85	0.47	< 0.6	php	3.8	[95]	$\pi^+\pi^-$
			ρ	32 ÷ 167	67	3 ÷ 50	6.2	< 0.6		6.0	[95]	$\pi^+\pi^-$
z6	[31]	2007	ρ	32 ÷ 180	90	2 ÷ 160		< 1		120	[96 – 00]	$\pi^+\pi^-$
h1c	[32]	2002	ρ	25 ÷ 70	38.1	< 1	10^{-4}	.073 ÷ .45	php	3	[99]	$\pi^+\pi^-$
h17	[33]	1999	ρ	30 ÷ 140	75	1 ÷ 5		< 0.5		0.125	[95]	$\pi^+\pi^-$
						2.5 ÷ 60				3.87	[96]	
z21	[34]	1997	ρ	50 ÷ 100	71.7	< 4	4×10^{-6}	< 0.5	php	2.17[b]	[94]	$\pi^+\pi^-$
z1d	[35]	1997	ρ	50 ÷ 100	72	< 4	10^{-5}	< 0.5	php	0.691	[94]	$\pi^+\pi^-$
z25	[36]	1996	ρ	50 ÷ 100	70	< 1	10^{-4}	.073 ÷ .4	php	0.898	[94]	$\pi^+\pi^-$
h22	[37]	1996	ρ	40 ÷ 80	55	< 0.5	0.035	< 0.5	php	0.0198	[93 – 94]	$\pi^+\pi^-$
			ρ	164 ÷ 212	187	< 0.01	0.001		php	0.0238	[93 – 94]	
z29	[38]	1995	ρ	60 ÷ 80	70	< 4	10^{-4}	< 0.5	php	0.55	[93]	$\pi^+\pi^-$
h2	[39]	2009	γ	30 ÷ 140	82	6.5 ÷ 80	10	< 1		306	[04 – 07]	
z5	[40]	2008	γ	40 ÷ 170	104	> 1.5	3.2	.08 ÷ .53		61.1	[99 – 00]	
h4	[41]	2007	γ	30 ÷ 140	82	6.5 ÷ 80	8	< 1		145	[05 – 06]	
h7	[42]	2005	γ	30 ÷ 140	82	2 ÷ 80	8	< 1		46.5	[96 – 00]	
z10	[43]	2003	γ	40 ÷ 140	89	5 ÷ 100	9.6			111.7	[96 – 00]	
h13	[44]	2001	γ	30 ÷ 120	75	2 ÷ 20	4.5	< 1		8		

(Table continued)

TABLE II. (*Continued*).

Index	Cite	Year	Low Energy (photoproduction) Particles	W (GeV)	$\lvert t\rvert$ (GeV^2)	Decay mode
f1	[48]	1979	ω	10.3 ÷ 18.4		
f2	[49]	1979	ρ, ϕ	7.6 ÷ 18.4		$\rho \to \pi^+\pi^-$, $\phi \to K^+K^-$
f3	[50]	1993	J/ψ	15.8 ÷ 26.5	< 1.5	$J/\psi \to \mu^+\mu^-$
sl1	[51]	1971	ρ	2.15 ÷ 4.0	.06 ÷ .8	$\rho \to \pi^+\pi^-$
c1	[52]	1982	ρ, ω	6.2 ÷ 9.2	.06 ÷ 1	$\rho \to \pi^+\pi^-$, $\omega \to \pi^+\pi^0\pi^-$
c2	[53]	1983	ϕ, ω	6.2 ÷ 11.5	< 1	$\phi, \omega \to \pi^+\pi^-\pi^0$
z2d	[54]	1997	ω, ϕ, ρ	9.2 ÷ 17.2		

[a]"php" stands for photoproduction.
[b]Luminosity after trigger selection.

Finally, we notice that amplitude (10) can be rewritten in the form

$$A(s,t,Q^2,M_V{}^2) = \widetilde{A}_s e^{-i\frac{\pi}{2}\alpha_s(t)}\left(\frac{s}{s_0}\right)^{\alpha_s(t)} e^{b_s t - n_s \ln\left(1+\frac{\widetilde{Q^2}}{Q_s^2}\right)} + \widetilde{A}_h e^{-i\frac{\pi}{2}\alpha_h(t)}\left(\frac{s}{s_0}\right)^{\alpha_h(t)} e^{b_h t-(n_h+1)\ln\left(1+\frac{\widetilde{Q^2}}{Q_h^2}\right)+\ln\left(\frac{\widetilde{Q^2}}{Q_h^2}\right)}, \quad (13)$$

where the two exponential factors $e^{b_s t - n_s \ln\left(1+\frac{\widetilde{Q^2}}{Q_s^2}\right)}$ and $e^{b_h t-(n_h+1)\ln\left(1+\frac{\widetilde{Q^2}}{Q_h^2}\right)+\ln\left(\frac{\widetilde{Q^2}}{Q_h^2}\right)}$ can be interpreted as the product of the form factors of upper and lower vertices (see Fig. 1c). It is interesting to remark that the amplitude (13) resembles the scattering amplitude in Ref. [5].

B. Fitting the two-component Pomeron to VMP and DVCS data from HERA

1. Normalization of the data from different reactions

Before fitting our model to the available HERA experimental data on $d\sigma_{\rm el}/dt(t)$ and $\sigma_{\rm el}(Q^2,W)$ of VMP and DVCS reactions, it is necessary to normalize these data such that they lie on the same surface, i.e. give the same values of the cross sections for the same values of W, $\widetilde{Q^2}$ (and t). We chose the J/ψ production as a "reference point." The normalization procedure is not unique. For example, according to Ref. [46] there are three sets of normalization parameters. For vector mesons in our calculations we used

$$f_{\rho^0}^{-1} : f_\omega^{-1} : f_\phi^{-1} : f_{J/\psi}^{-1} : f_\Upsilon^{-1} = 0.68 : 0.068 : 0.155 : 1 : 0.75. \quad (14)$$

The f_Υ was found from the fit.

Let us stress that we compared the data for different reactions at the same values of $\widetilde{Q^2}$, rather than Q^2.

After normalization, the differential and elastic cross sections lie on the same surface, so that

$$f_{\rho^0}\sigma_{\rho^0} = f_\omega\sigma_\omega = f_\phi\sigma_\phi = f_{J/\psi}\sigma_{J/\psi} = f_\Upsilon\sigma_\Upsilon,$$

where each σ stands for all kinds of cross section. Just as an example, the fit of Eq. (12) to the normalized data on cross section $f_i \cdot \sigma_{\rm el}(\widetilde{Q^2})$ relative to ρ^0, ω, ϕ and J/ψ production is shown in Fig. 3.

2. Fitting procedure

We performed a global fit of our model, using Eqs. (11) and (12), to all elastic exclusive VMP (i.e. ρ^0, ω, ϕ, J/ψ and Υ) [11–39] and DVCS HERA data [40–44], with $W > 30$ GeV. The compiled information about the data can be found in Tables II and II (continued) [we remind that low W were not used in the fitting, but are present on the figures]. Notice that in this energy range only diffractive events were selected at HERA and, consequently, the Pomeron is the only object exchanged in the t channel.

The fitting strategy is based on the minimization of the quantity $\tilde{\chi}^2 = \frac{1}{N}\sum_{i=1}^{N}\tilde{\chi}_i^2$, where N is the number of all reactions involved (i.e. ρ, ϕ, ω, J/ψ, Υ and γ production), i numerate a class of reaction; $\tilde{\chi}_i$ is the mean value of χ^2 for different types of data for selected class of reactions, defined as $\tilde{\chi}_i = \frac{1}{N_i}\sum_{k=1}^{N_i}\tilde{\chi}_{k,i}^2$, where $\tilde{\chi}_{k,i}^2$ is $\chi_{k,i}^2/d.o.f.$ for ith class of reactions and kth type of data, i.e. those relative to $\sigma_{\rm el}(Q^2)$, $\sigma_{\rm el}(W)$ and $d\sigma_{\rm el}(t)/dt$; N_i is number of different type of data for ith class of reactions.

Following relation (14), we fixed the normalization parameters at

$$f_\rho^{-1} = 0.680, \quad f_\phi^{-1} = 0.155, \quad f_\omega^{-1} = 0.068, \quad f_{J/\psi}^{-1} = 1, \quad f_\Upsilon^{-1} = 0.750, \quad (15)$$

and set s_0 equal to 1 GeV^2.

DVCS and VMP are similar in the sense that in both reactions a vector particle is produced. However there are

differences between the two because of the vanishing rest mass of the produced real photon. The unified description of these two types of related reactions does not work by simply setting $M_\gamma = 0$. From fits we found $M^{\rm eff}_{\rm DVCS} = 1.8$ GeV and a normalization factor $f^{-1}_{\rm DVCS} = 0.091$ follows.

The "effective DVCS mass" resulting from the fits to DVCS appears large, indicating that the unified description of vector meson production $\gamma^* p \to V p$ and Compton scattering $\gamma^* p \to \gamma p$ may not be that simple. The first reason for this abnormal value is technical, related to our neglect of the contribution from secondary trajectories, fully justified, due to the Zweig (OZI) rule in the case of e.g. ϕ or J/ψ production, but important in Compton scattering. Another reason may be conceptual, related to the twin role of the photon: real photon production (Compton scattering) may imply a zero photon mass, but, on the other hand, by vector meson dominance the produced photon's wave function contains a superposition of vector mesons' wave functions expressed by

$$A^{\gamma p\to\gamma p} = \sum_{V=\rho^0,\omega,\phi,\ldots} \frac{\sqrt{4\pi\alpha_{em}}}{g_V} A^{\gamma p\to V p},$$

[see [46], Eq. (184)], which leads to the so-called Stodolsky sum rule [47]

$$\sigma_{tot}(\gamma p) = \sqrt{16\pi \frac{d\sigma^{\gamma p\to\gamma p}}{dt}\Big|_{t=0}} = \sum_{V=\rho^0,\omega,\phi,\ldots} \sqrt{16\pi \frac{4\pi\alpha_{em}}{g_V^2} \frac{d\sigma^{\gamma p\to V p}}{dt}\Big|_{t=0}}.$$

This may lead to the nonzero effective DVCS mass parameter. A better understanding of DVCS needs further, in particular experimental, studies of both real and virtual Compton scattering.

The results of the fit are shown in Fig. 3 [for $\sigma_{\rm el}(\widetilde{Q^2})$], in Figs. 4–6 [for $\sigma_{\rm el}(W)$] and Figs. 7–10 [for $d\sigma_{\rm el}(t)/dt$] for vector meson production, and in Figs. 11–12 for DVCS, with the values of the fitted parameters given in Table III. The mean value of the total $\tilde{\chi}^2$ (see its definition above) is equal to 0.986. The mean values of $\tilde{\chi}^2$ of the fit for different observables [i.e. $\sigma_{\rm el}(Q^2)$, $\sigma_{\rm el}(W)$ or $d\sigma_{\rm el}(t)/dt$] and different reactions (VMP or DVCS), together with the numbers of degrees of freedom (number of data points) and the global mean value $\tilde{\chi}^2_i$, are shown in Table IV. Furthermore, in Table V the parameters of the two-component Pomeron model [Eqs. (11) and (12)] fitted to the combined VMP and DVCS data are quoted, when Pomeron trajectories are fixed to $\alpha_s(t) = 1.08 + 0.25t$ and $\alpha_h(t) = 1.20 + 0.01t$.

Next, by using Eq. (11) with the values of the parameters from Table III and the formula

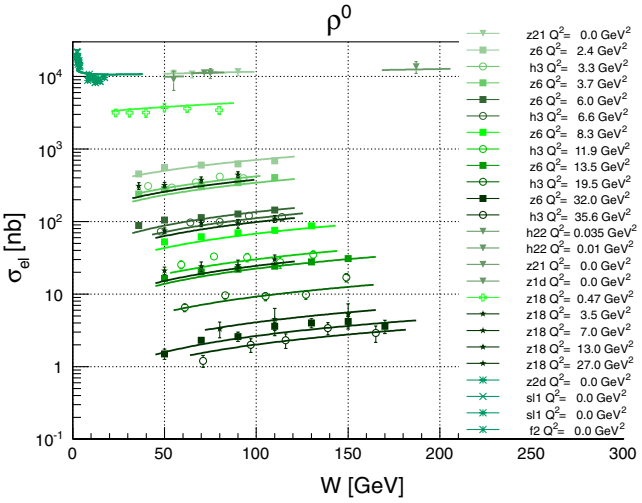

FIG. 4 (color online). Fit of Eq. (12) to the data on the elastic cross section $\sigma_{\rm el}(W)$ for ρ^0, for different values of Q^2.

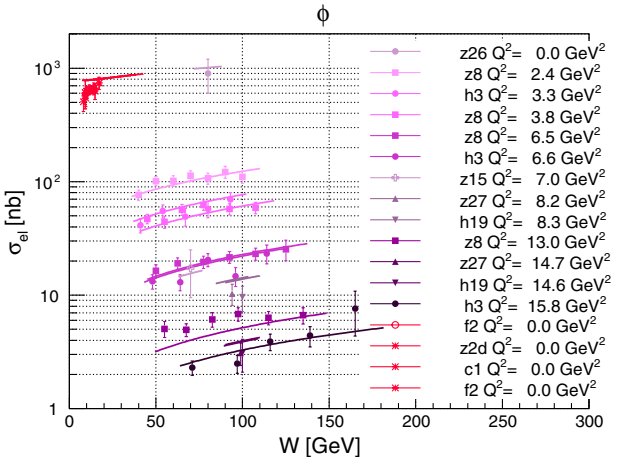

FIG. 5 (color online). Fit of Eq. (12) to the data on the elastic cross section $\sigma_{\rm el}(W)$ for ϕ, for different values of Q^2.

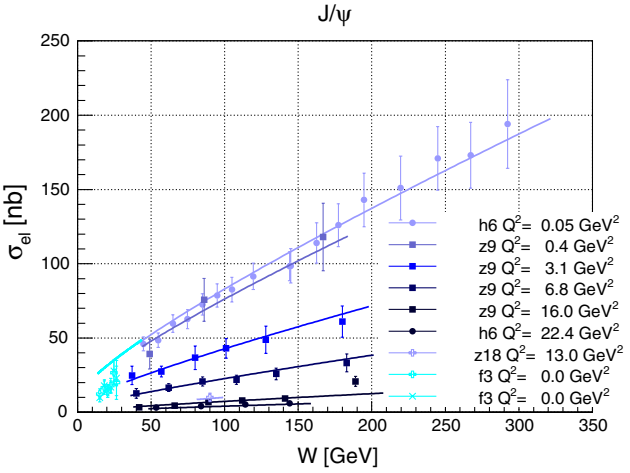

FIG. 6 (color online). Fit of Eq. (12) to the data on the elastic cross section $\sigma_{\rm el}(W)$ for J/ψ, for different values of Q^2.

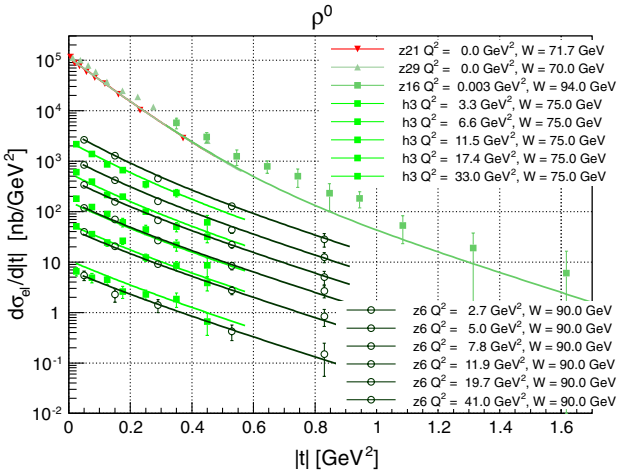

FIG. 7 (color online). Fit of Eq. (11) to the data on the differential elastic cross section $d\sigma_{\rm el}/dt$ for ρ^0 as a function of Q^2 and W.

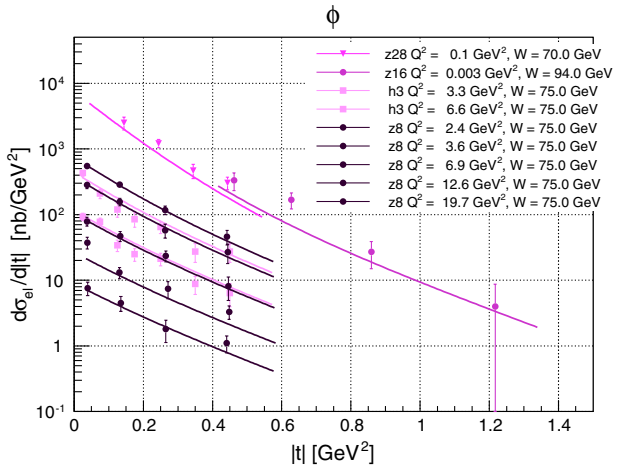

FIG. 8 (color online). Fit of Eq. (11) to the data on the elastic differential cross section $d\sigma_{\rm el}/dt$ for ϕ as a function of Q^2 and W.

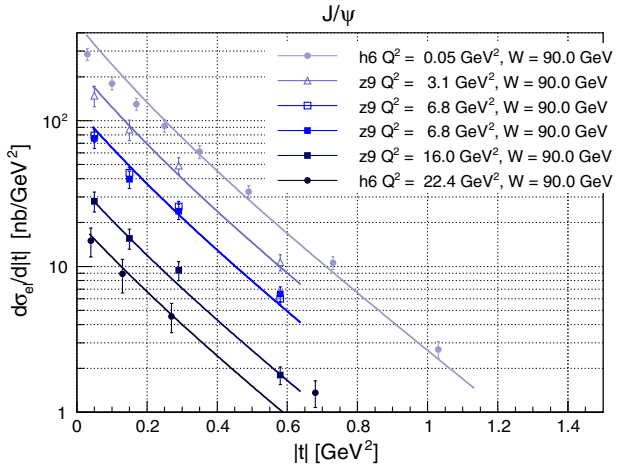

FIG. 9 (color online). Fit of Eq. (11) to the data on the elastic differential cross section $d\sigma_{\rm el}/dt$ for J/ψ, for different values of Q^2 and $W = 90$ GeV.

$$B(Q^2, W, t) = \frac{d}{dt} \ln \frac{d\sigma_{\rm el}}{dt}, \tag{16}$$

we calculate the forward slopes and compare them with the experimental data on VMP, including those for the Ψ (2S) production. To do so, the experimental data were grouped in four separate t bins with the mean values of 0.12, 0.25, 0.5 and 0.6 GeV^2. The results of these calculations, showing the $\widetilde{Q^2}$ dependence, are presented in Fig. 13. A compilation of all results is presented in Fig. 14. In Figs. 13–14 the results on Ψ (2S) slope are also shown.

As seen from Figs. 3–12 and Tables III,IV,V, the overall fit to the large number of the diffractive data by the two-component Pomeron amplitude (Eq. (10) is impressive, apart from some peculiar cases. In particular, two points need to be better understood

(i) the compatibility of VMP and DVCS (the problem with effective DVCS mass),
(ii) some minor problems of the description of J/ψ production in the region of low t and Q^2.

The number of the fitted parameters of the two-component Pomeron model [Eq. (15)] is 12 (Table III), with five additional normalization factors for six vector particle productions: ρ^0, ϕ, ω, J/ψ, Υ and γ ($f_{J/\psi} = 1$ is not taking into account since it is the baseline of our normalization). If we fix the Pomeron trajectories $\alpha_s(t)$ and $\alpha_h(t)$ (see Table V), the number of free parameters reduces to 8. In the case of a single-component Pomeron (see Sec. II) the number of parameters for five different types reactions was much larger: $7 \times 5 = 35$ (see Table I).

IV. BALANCING BETWEEN THE SOFT AND HARD DYNAMICS

In this section we illustrate the important and delicate interplay between the soft and hard components of our unique Pomeron. Since the amplitude consists of two parts, according to the definition (1), it can be written as

$$A(Q^2, s, t) = A_s(Q^2, s, t) + A_h(Q^2, s, t). \tag{17}$$

As a consequence, the differential and elastic cross sections contain also an interference term between soft and hard parts, so that they read

$$\frac{d\sigma_{\rm el}}{dt} = \frac{d\sigma_{s,\rm el}}{dt} + \frac{d\sigma_{h,\rm el}}{dt} + \frac{d\sigma_{\rm interf,el}}{dt}, \tag{18}$$

and

$$\sigma_{\rm el} = \sigma_{s,\rm el} + \sigma_{h,\rm el} + \sigma_{\rm interf,el}, \tag{19}$$

according to Eqs. (11) and (12), respectively.

Using Eqs. (18) and (19), we can define the following ratios for each component: $R_i(\widetilde{Q^2}, W, t) = \frac{d\sigma_{i,\rm el}}{dt} / \frac{d\sigma_{\rm el}}{dt}$, and $R_i(\widetilde{Q^2}, W) = \sigma_{i,\rm el}/\sigma_{\rm el}$, where i stands for $\{s, h, interf\}$.

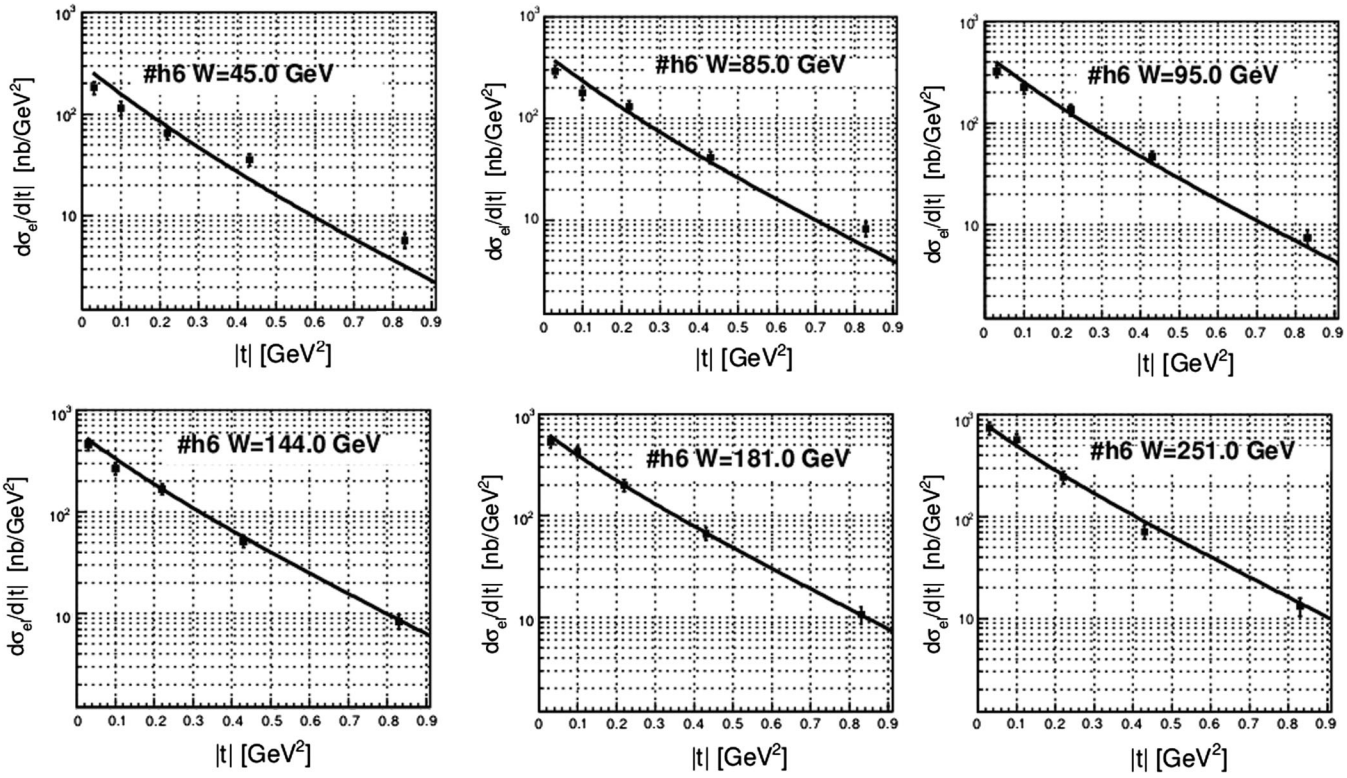

FIG. 10. Fit of Eq. (11) to the data on the elastic differential cross section $d\sigma_{\rm el}/dt$ for J/ψ at photoproduction ($Q^2 = 0.05$ GeV^2), for different values of W.

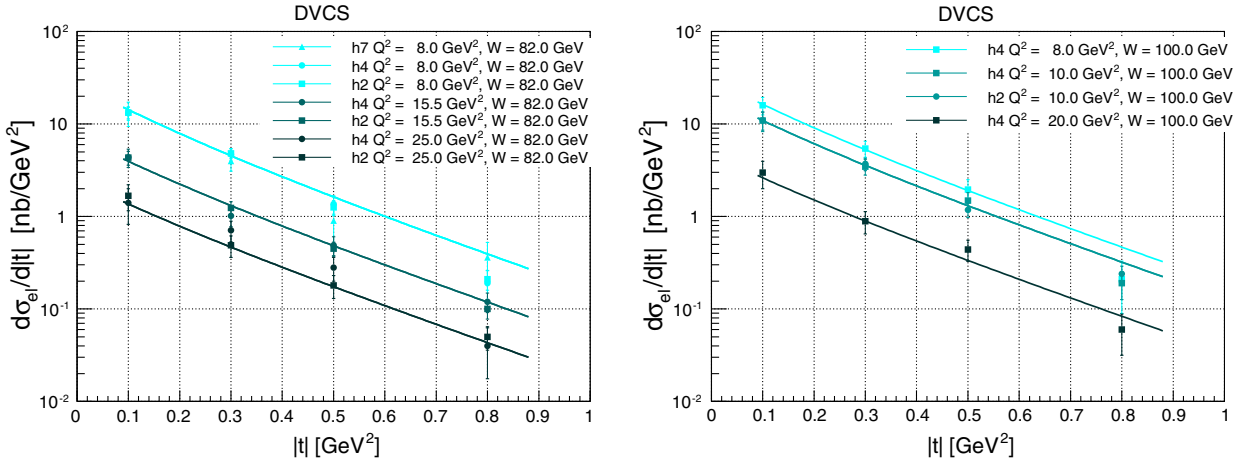

FIG. 11 (color online). Fit of Eq. (11) to the data on the elastic differential cross section $d\sigma_{\rm el}/dt$ for DVCS.

Figure 15 shows the interplay between the components for both $\sigma_{i,\rm el}$ and $R_i(\widetilde{Q^2}, t)$, as functions of $\widetilde{Q^2}$, for $W = 70$ GeV. In Fig. 16 both plots show that not only is $\widetilde{Q^2}$ the parameter defining softness or hardness of the process, but such is also the combination of $\widetilde{Q^2}$ and t, similar to the variable $z = t - Q^2$ introduced in Ref. [5]. On the whole, it can be seen from the plots that the soft component dominates in the region of low $\widetilde{Q^2}$ and t, while the hard component dominates in the region of high $\widetilde{Q^2}$ and t.

As expected, the soft term dominates at low values of $\widetilde{Q^2}$, replaced by the hard one at high $\widetilde{Q^2}$ (Fig. 15). The contribution from the interference term is considerable, however it remains below the first two (except for

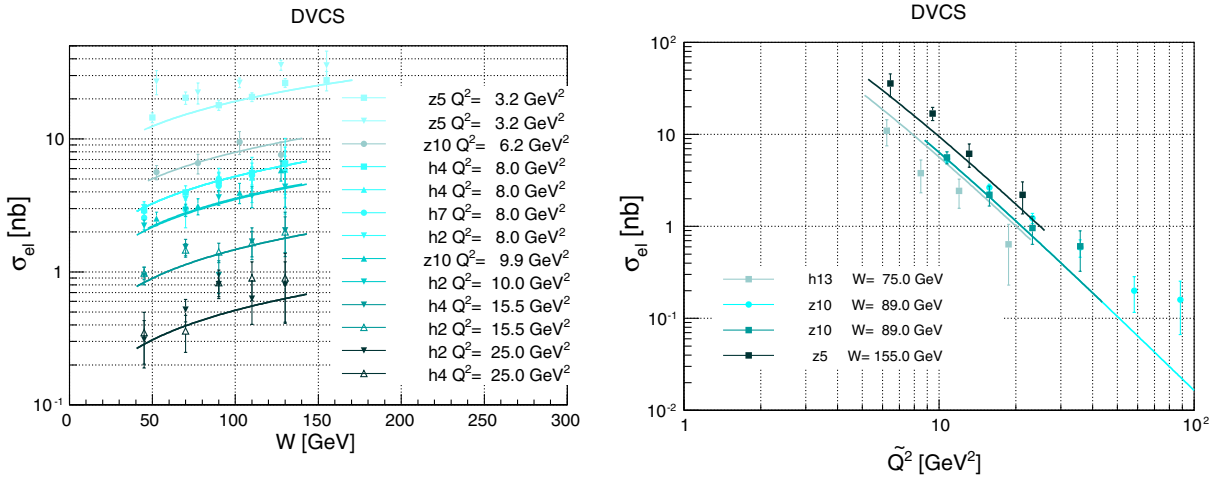

FIG. 12 (color online). Fit of Eq. (12) to the data on the elastic cross section $\sigma_{\rm el}$ for DVCS.

intermediate values of $\widetilde{Q^2}$). The account for absorption corrections (shadowing, neglected in the present study) is expected to suppress the contribution from the interference term.

V. HADRON-INDUCED REACTIONS: HIGH-ENERGY *PP* SCATTERING

Hadron-induced reactions differ from those induced by photons at least in two aspects. First, hadrons are on the

TABLE III. Parameters of the two-component Pomeron model, Eqs. (11) and (12), fitted to the combined VMP and DVCS data. The $\tilde{\chi}^2$ value equals 0.986.

	$A_{0s,h}\,(\frac{\sqrt{\rm nb}}{\rm GeV})$	$\widetilde{Q^2_{s,h}}\,({\rm GeV}^2)$	$n_{s,h}$	$\alpha_{0s,h}$	$\alpha'_{s,h}\,(\frac{1}{\rm GeV^2})$	$b_{s,h}\,(\frac{1}{\rm GeV^2})$
soft	2104 ± 1749	0.29 ± 0.20	1.63 ± 0.40	1.005 ± 0.090	0.32 ± 0.57	2.93 ± 5.06
hard	44 ± 22	1.15 ± 0.52	1.34 ± 0.16	1.225 ± 0.055	0.0 ± 17	2.22 ± 3.09

TABLE IV. Values of $\tilde{\chi}^2$ of the fit and the numbers of degrees of freedom (number of data points) for different observables [i.e. $\sigma_{\rm el}(W)$, $\sigma_{\rm el}(Q^2)$ or $d\sigma_{\rm el}(t)/dt$], and values of $\tilde{\chi}^2_i$ for different reactions (VMP or DVCS).

Meson production	$\sigma_{\rm el}(W)$ $\tilde{\chi}^2$	$N_{d.o.f}$	$\sigma_{\rm el}(Q^2)$ $\tilde{\chi}^2$	$N_{d.o.f}$	$\frac{d\sigma_{\rm el}}{dt}$ $\tilde{\chi}^2$	$N_{d.o.f}$	average $\tilde{\chi}^2_i$
Υ	0.47	4	0.00	1	0.00	1	0.469
$J\psi$	0.47	43	0.47	16	2.37	92	1.105
ω	0.10	3	0.09	4	0.33	7	0.174
ϕ	1.19	46	1.42	22	1.10	85	1.238
ρ	1.49	112	0.97	64	3.85	94	2.104
DVCS	1.83	89	2.20	38	1.41	84	1.815

TABLE V. Parameters of the two-component Pomeron model, Eqs. (11) and (12), fitted to the combined VMP and DVCS data, with fixed parameters of the Pomeron trajectories $\alpha_s(t) = 1.08 + 0.25t$ and $\alpha_h(t) = 1.20 + 0.01t$.

	$A_{0s,h}\,(\frac{\sqrt{\rm nb}}{\rm GeV})$	$\widetilde{Q^2_{s,h}}\,({\rm GeV}^2)$	$n_{s,h}$	$\alpha_{0s,h}$	$\alpha'_{s,h}\,(\frac{1}{\rm GeV^2})$	$b_{s,h}\,(\frac{1}{\rm GeV^2})$
soft	807 ± 1107	0.46 ± 0.70	1.79 ± 0.79	1.08	0.25	3.41 ± 2.48
hard	47.9 ± 46.9	1.30 ± 1.12	1.33 ± 0.26	1.20	0.01	2.15 ± 1.14

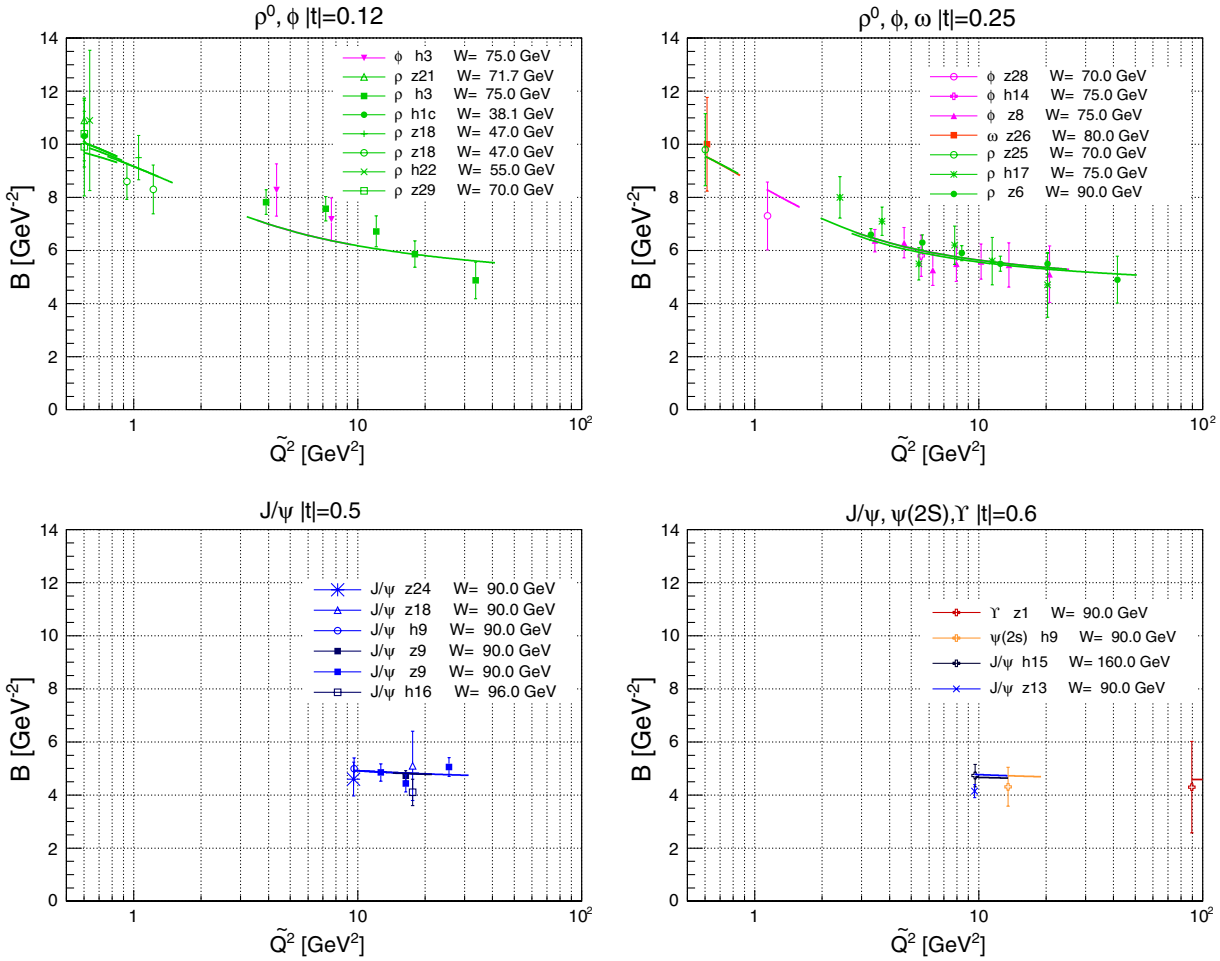

FIG. 13 (color online). Experimental data on the slope B as a function of $\widetilde{Q^2}$ for $\rho^0, \phi, J/\psi$ Υ, and Ψ (2S) at $|t| = 0.12$, 0.25, 0.5, 0.6 GeV^{-2}, and our theoretical predictions coming from Eq. (16).

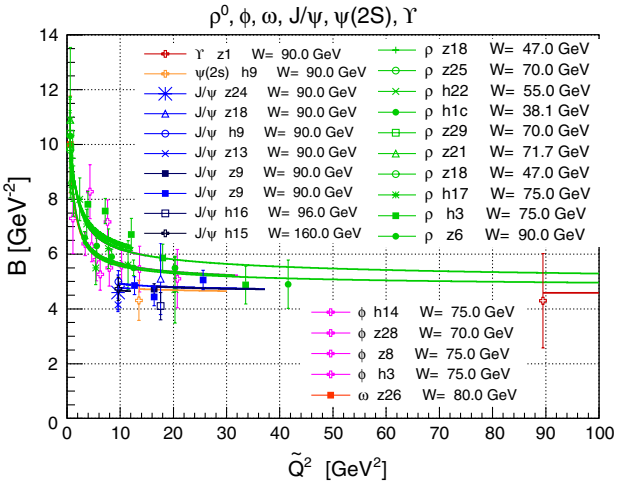

FIG. 14 (color online). Experimental data on the slope B as a function of $\widetilde{Q^2}$ for $\rho^0, \phi, J/\psi$ Υ, and Ψ (2S), and our theoretical predictions coming from Eq. (16).

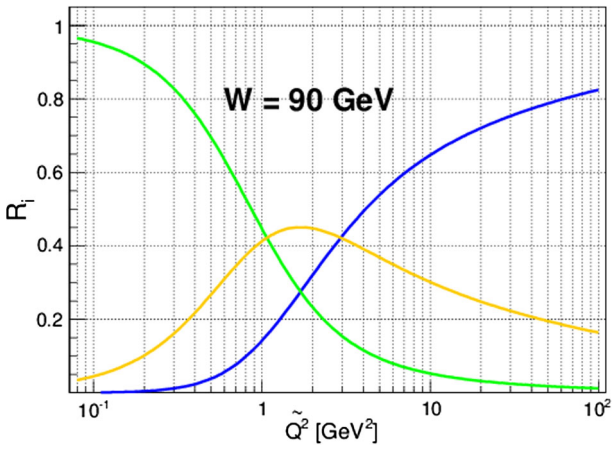

FIG. 15 (color online). Partial value $R_i(\widetilde{Q^2}, W)$ of soft (green line, low $\widetilde{Q^2}$), hard (blue line, high $\widetilde{Q^2}$) and interference (yellow line, moderate $\widetilde{Q^2}$) components of cross section, at $W = 70$ GeV.

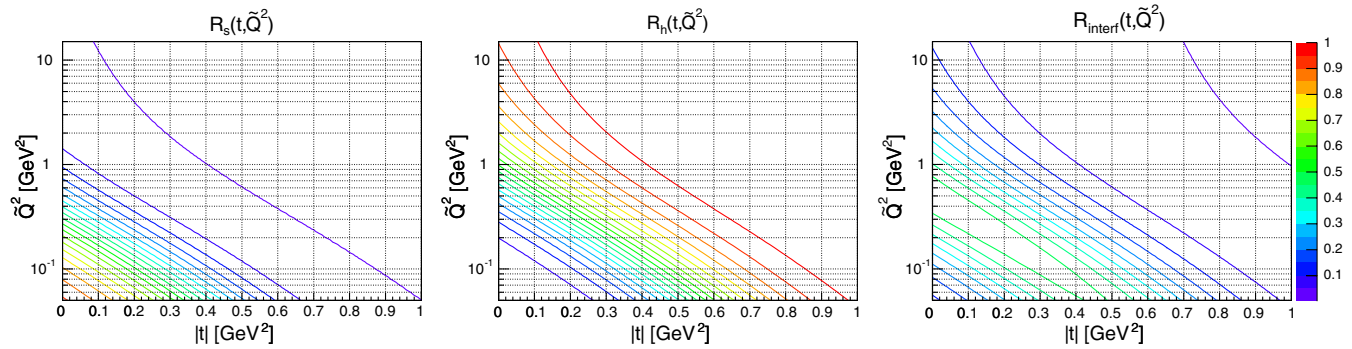

FIG. 16 (color online). Soft, hard and interference components of the ratio $R_i(\widetilde{Q^2}, W, t)$ are shown as functions of $\widetilde{Q^2}$ and t, for $W = 70$ GeV.

mass shell and hence the relevant processes are typically soft. Second, the mass of incoming hadrons is positive, while the virtual photon has negative squared "mass." Our attempt to include hadron-hadron scattering into the analysis with our model has the following motivations: (i) by vector meson dominance (VMD) the photon behaves partly as a meson, therefore meson-baryon (and more generally, hadron-hadron) scattering has much in common with photon-induced reactions. Deviations from VMD may be accounted for the proper Q^2 dependence of the amplitude (as we do hope is in our case); (ii) of interest is the connection between space- and timelike reactions; (iii) according to recent claims (see e.g. Ref. [9,45]) the highest-energy (LHC) proton-proton scattering data indicate the need for a hard component in the Pomeron (to anticipate, our fits do not support the need of any noticeable hard component in pp scattering).

We did not intend to make a high-quality fit to the pp data; that would be impossible without the inclusion of subleading contributions and/or the Odderon. Instead we normalized the parameters of our leading Pomeron term according to recent fits by Donnachie and Landshoff [9] including, apart from a soft term, also a hard one.

The pp scattering amplitude is written in the form similar to the amplitude (10) for VMP or DVCS, the only difference being that the normalization factor is constant since the pp scattering amplitude does not depend on Q^2:

$$A^{pp}(s,t) = A_s^{pp} e^{-i\frac{\pi}{2}\alpha_s(t)} \left(\frac{s}{s_0}\right)^{\alpha_s(t)} e^{b_s t} + A_h^{pp} e^{-i\frac{\pi}{2}\alpha_h(t)} \left(\frac{s}{s_0}\right)^{\alpha_h(t)} e^{b_h t}. \quad (20)$$

We fixed the parameters of Pomeron trajectories in accord with those of Refs. [9,59]

$$\alpha_s(t) = 1.084 + 0.35t, \qquad \alpha_h(t) = 1.30 + 0.10t.$$

With these trajectories the total cross section

$$\sigma_{\text{tot}} = \frac{4\pi}{s} ImA(s,t)|_{t=0}, \quad (21)$$

was found to be compatible with the LHC data, as seen on Fig. 17(a). From the comparison of Eq. (21) to the LHC data we get

$$A_s^{pp} = -1.73\text{mb} \cdot \text{GeV}^2, A_h^{pp} = -0.0012\text{mb} \cdot \text{GeV}^2.$$

The parameter b_s was determined by fitting the differential and integrated elastic cross sections to the data taken from Refs. [55–58]. To this aim, we used Eqs. (11) and (12), the normalization factors H_s and H_h replaced with A_s^{pp} and A_h^{pp}, respectively, according to Eq. (20). The parameter b_h, was set to be equal to b_s, since for DVCS and VMP these parameters assume similar values, as seen from in Tables III and V. By adjusting the theoretical curves to the data, we get $b_s = b_h = 1.8\ \text{GeV}^{-2}$. The comparison with the experimental data from Refs. [55,57,58] is shown in Fig. 17(b) for the integrated cross section and in Fig. 18(a) for the differential elastic cross section.

Next, by using formula (16) we calculated the forward slope B, shown in Fig. 18(b) together with data from Refs. [55] and [58,60].

From these figures we conclude that, while the data on the total cross section is compatible with a small hard admixture in the amplitude, the slope parameter with a hard component included seems to manifest a wrong tendency, by slowing down with increasing energy, while the TOTEM measurements [55] show the contrary.

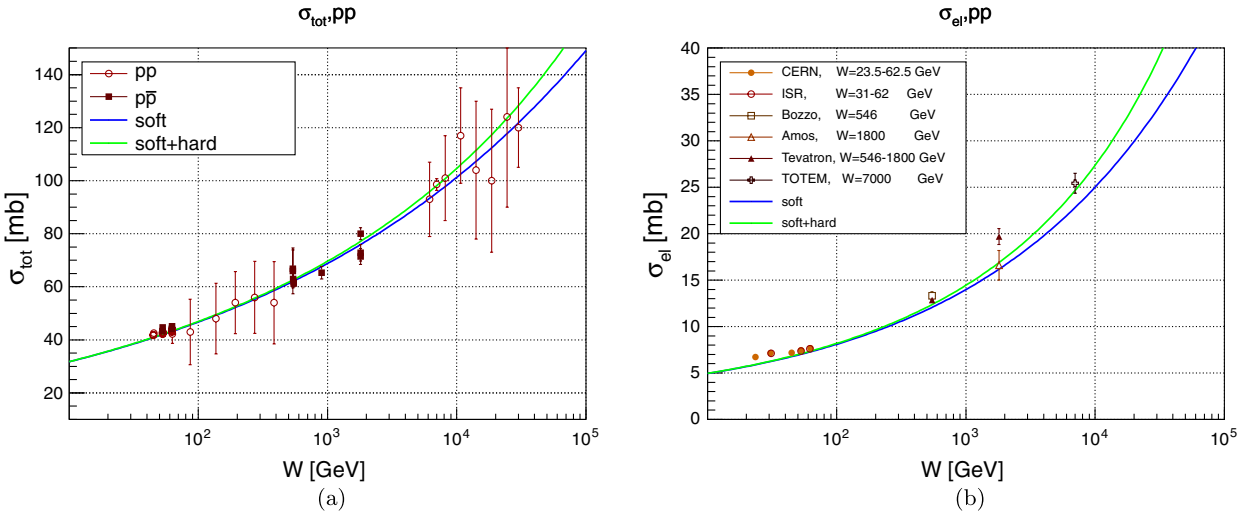

FIG. 17 (color online). (a) The total $\sigma_{\rm tot}(W)$ and (b) the elastic cross sections $\sigma_{\rm el}(W)$ for pp scattering. The data are taken from Refs. [55–58].

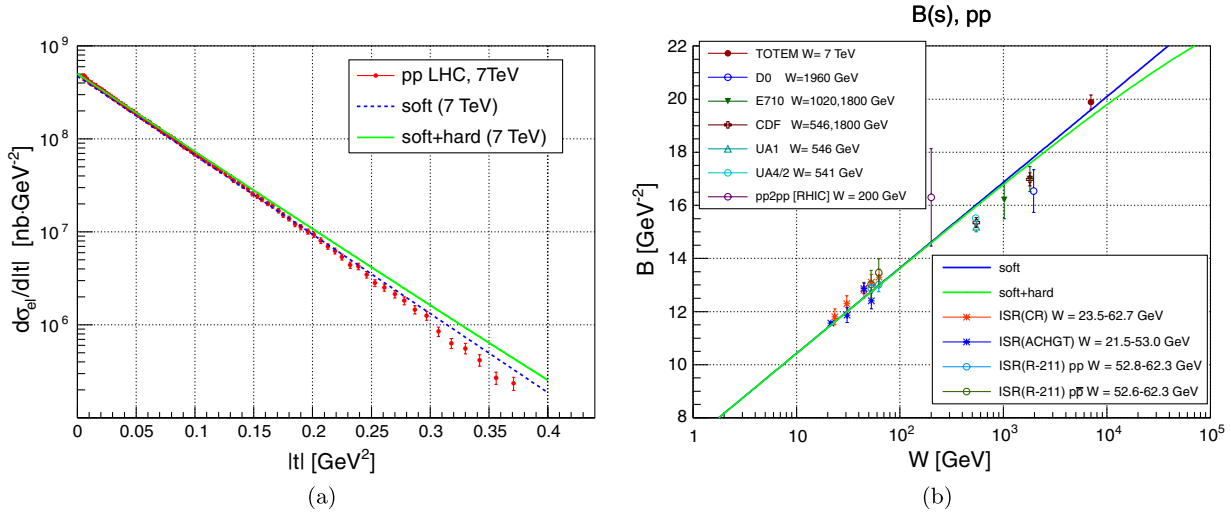

FIG. 18 (color online). (a) The differential elastic cross section $d\sigma_{\rm el}/dt$ for pp-scattering. (b) The slope, B, of the differential elastic cross section for pp-scattering as a function of W. The data are from Refs. [55,58,60].

VI. DISCUSSION OF THE RESULTS AND CONCLUSIONS

In this paper we have proposed an economic model describing both soft and hard exclusive production of vector particles. It features a unique, "universal" Pomeron, same for all processes. This Pomeron is made of two terms, a soft and a hard component, their relative weight depending on the softness or hardness of the given processes.

The model incorporates some features of earlier models Refs. [4,5,7], such as the interplay between the dependence of the scattering amplitude on the virtuality Q^2 and the squared momentum transfer t.

In the framework of the model we have analyzed all available data on vector meson [ρ^0, ω, ϕ, J/ψ, Υ, Ψ (2S)] production and DVCS obtained at HERA by the H1 and ZEUS Collaborations. A global fit was performed with a small number of free parameters, namely eight parameters: four parameters of Pomeron trajectories and five parameters for the normalization of the cross sections in six processes, universal for all reactions. By fixing the parameters of the Pomeron trajectories, their number reduces to six. The results of the fit are presented in Figs. 3 [$\sigma_{\rm el}(\widetilde{Q^2})$], Figs. 4–6 [$\sigma_{\rm el}(W)$], Figs. 7–10 [$d\sigma_{\rm el}(t)/dt$] and Figs. 13–14 (the slope B) for VMP and in Figs. 11–12 for DVCS. The values of the parameters are quoted in Tables III and V.

The resulting fit is reasonable, despite the following minor problems:

(i) in order to incorporate DVCS together with VMP, we need to assign some nonzero value to the mass of the real photon, that can be treated as an effective mass of quark-antiquark system into which the virtual photon fluctuates. From the fit we obtained $M^{\rm eff}_{\rm DVCS} = 1.8$ GeV;

(ii) there are some systematic shifts of theoretical curves with respect to the experimental data in the regions of low Q^2, W and t for the J/ψ fit (see Figs. 6, 9 and 10). This effect may come both from the absence of the secondary Reggeons, and from the influence of the soft (and/or the interference) term of the elastic cross section $\sigma_{\rm el}(Q^2, W, t)$;

Among the remaining open problems, to be treated in subsequent studies, are

(i) the present paper we have neglected subleading Regge contributions. They must be included in any extension of the model to lower energies (below 30 GeV);

(ii) $\widetilde{Q^2}$ dependence of the scattering amplitude introduced in the present paper empirically has to be compared with the results of unitarization and/or QCD evolution. We intend to come back to this point in the future;

(iii) seen from Sec. IV, the soft component of the Pomeron dominates in the region of small $|t|$ and small $\widetilde{Q^2}$.

Hence, a parameter, responsible for the softness and/or hardness of processes, should be a combination of t and Q^2. A simple solution was suggested in Ref. [5] with the introduction of the variable $z = t - Q^2$. The interplay of these two variables remains an important open problem that requires further investigation.

The extension of our formalism to hadronic reactions (pp scattering) shows that the available data can be described by a single, soft, component.

ACKNOWLEDGMENTS

L. J. thanks the Dipartimento di Fisica dell'Università della Calabria and the Istituto Nazionale di Fisica Nucleare—Gruppo Collegato di Cosenza, where part of this work was done, for their hospitality and support. He was supported partly also by the grant "Matter under extreme conditions" of the National Academy of Sciences of Ukraine, Dept. of Astronomy and Physics, and by the DOMUS Curatorium of the Hungarian Academy of Sciences.

[1] V. S. Fadin, E. Kuraev, and L. Lipatov, Phys. Lett. **60B**, 50 (1975); I. Balitsky and L. Lipatov, Sov. J. Nucl. Phys. **28**, 822 (1978).

[2] V. Barone and E. Predazzi, *High-Energy Particle Diffraction* (Springer, New York, 2002), p. 1.

[3] S. Donnachie, H. G. Dosch, O. Nachtmann, and P. Landshoff, *Pomeron Physics and QCD*, Cambridge Monographs on Particle Physics, Nuclear Physics, and Cosmology Vol. 19 (Cambridge University Press, Cambridge, England, 2002), pp. 347.

[4] S. Fazio, R. Fiore, A. Lavorini, L. Jenkovszky, and A. Salii, Acta Phys. Pol. B **44**, 1333 (2013).

[5] M. Capua, S. Fazio, R. Fiore, L. L. Jenkovszky, and F. Paccanoni, Phys. Lett. B **645**, 161 (2007).

[6] R. Fiore, L. L. Jenkovszky, and F. Paccanoni, Eur. Phys. J. C **10**, 461 (1999).

[7] S. Fazio, R. Fiore, L. Jenkovszky, and A. Lavorini, Phys. Rev. D **85**, 054009 (2012).

[8] S. Fazio, R. Fiore, L. Jenkovszky, A. Lavorini, and A. Saliy, in *Proceedings of 14th Workshop on Elastic and Diffractive Scattering (EDS Blois Workshop) on Frontiers of QCD: From Puzzles to Discoveries*, edited by M. A. Rotondo and C.-I. Tan (Quy Nhon, Vietnam, 2011); http://www.slac.stanford.edu/econf/C111215/; L. Jenkovszky, A. Salii, and V. Batozskaya, in *Proceedings of QUARKS-2012, 17th International Seminar on High Energy Physics* (Yaroslavl, Russia, 2012); L. Jenkovszky, A. Salii, J. Turóci, and D. Himics, in *Proceedings of "The 4th International Conference Current Problems in Nuclear Physics and Atomic Energy (NPAE-2012)"* (Kyiv, Ukraine, 2012), Vol. 1; R. Fiore, L. Jenkovszky, A. Lavorini, and A. Salii, in *Proceedings of 7th International Workshop on Diffraction in High Energy Physics (Diffraction 2012)*, edited by M. Capua, R. Fiore, A. Papa, A. Sabio Vera, and E. Tassi (Puerto del Carmen, Lanzarote, Canary Islands, Spain, 2012); R. Fiore, L. Jenkovszky, A. Lavorini, and A. Salii, AIP Conf. Proc. **1523**, 83 (2013).

[9] P. V. Landshoff, Acta Phys. Pol. B **40**, 1967 (2009).

[10] A. Donnachie and P. Landshoff, arXiv:0803.0686.

[11] H. Abramowicz *et al.* (ZEUS Collaboration), Phys. Lett. B **708**, 14 (2012).

[12] S. Chekanov *et al.* (ZEUS Collaboration), Phys. Lett. B **680**, 4 (2009).

[13] J. Breitweg *et al.* (ZEUS Collaboration), Phys. Lett. B **437**, 432 (1998).

[14] C. Adloff *et al.* (H1 Collaboration), Phys. Lett. B **483**, 23 (2000).

[15] C. Adloff *et al.* (H1 Collaboration), Phys. Lett. B **541**, 251 (2002).

[16] A. Aktas *et al.* (H1 Collaboration), Eur. Phys. J. C **46**, 585 (2006).

[17] S. Chekanov *et al.* (ZEUS Collaboration), Nucl. Phys. **B695**, 3 (2004).

[18] S. Chekanov *et al.* (ZEUS Collaboration), Eur. Phys. J. C **24**, 345 (2002).

[19] C. Adloff *et al.* (H1 Collaboration), Eur. Phys. J. C **10**, 373 (1999).
[20] J. Breitweg *et al.* (ZEUS Collaboration), Z. Phys. C **75**, 215 (1997).
[21] J. Breitweg *et al.* (ZEUS Collaboration), Eur. Phys. J. C **14**, 213 (2000).
[22] F. Aaron *et al.* (H1 Collaboration), J. High Energy Phys. 05 (2010) 032.
[23] J. Breitweg *et al.* (ZEUS Collaboration), Phys. Lett. B **487**, 273 (2000).
[24] M. Derrick *et al.* (ZEUS Collaboration), Z. Phys. C **73**, 73 (1996).
[25] S. Chekanov *et al.* (ZEUS Collaboration), Nucl. Phys. **B718**, 3 (2005).
[26] C. Adloff *et al.* (H1 Collaboration), Phys. Lett. B **483**, 360 (2000).
[27] C. Adloff *et al.* (H1 Collaboration), Z. Phys. C **75**, 607 (1997).
[28] M. Derrick *et al.* (ZEUS Collaboration), Phys. Lett. B **377**, 259 (1996).
[29] M. Derrick *et al.* (ZEUS Collaboration), Phys. Lett. B **380**, 220 (1996).
[30] J. Breitweg *et al.* (ZEUS Collaboration), Eur. Phys. J. C **6**, 603 (1999).
[31] S. Chekanov *et al.* (ZEUS Collaboration), PMC Phys. A **1**, 6 (2007).
[32] H1 Collaboration, in *Proceedings of "31st International Conference on High Energy Physics (ICHEP 2002)"* (Elsevier, Amsterdam, The Netherlands, 2002) abstract 991, session 6, http://www.ichep02.nl/index-new.html; O. Karschnick, Ph.D. thesis, Universität Hamburg, 2001; Report No. DESY-THESIS-2001-026.
[33] C. Adloff *et al.* (H1 Collaboration), Eur. Phys. J. C **13**, 371 (2000).
[34] J. Breitweg *et al.* (ZEUS Collaboration), Eur. Phys. J. C **2**, 247 (1998).
[35] D. Westphal, Ph.D. thesis, Universität Hamburg, 1997; Report No. DESY-F35D-97-11.
[36] M. Derrick *et al.* (ZEUS Collaboration), Z. Phys. C **73**, 253 (1997).
[37] S. Aid *et al.* (H1 Collaboration), Nucl. Phys. **B463**, 3 (1996).
[38] M. Derrick *et al.* (ZEUS Collaboration), Z. Phys. C **69**, 39 (1995).
[39] F. Aaron *et al.* (H1 Collaboration), Phys. Lett. B **681**, 391 (2009).
[40] S. Chekanov *et al.* (ZEUS Collaboration), J. High Energy Phys. 05 (2009) 108.
[41] F. Aaron *et al.* (H1 Collaboration), Phys. Lett. B **659**, 796 (2008).
[42] A. Aktas *et al.* (H1 Collaboration), Eur. Phys. J. C **44**, 1 (2005).
[43] S. Chekanov *et al.* (ZEUS Collaboration), Phys. Lett. B **573**, 46 (2003).
[44] C. Adloff *et al.* (H1 Collaboration), Phys. Lett. B **517**, 47 (2001).
[45] A. Donnachie and P. Landshoff, arXiv:1112.2485.
[46] I. Ivanov, N. Nikolaev, and A. Savin, Phys. Part. Nucl. **37**, 1 (2006).
[47] L. Stodolsky, Phys. Rev. Lett. **18**, 135 (1967).
[48] R. Egloff, P. Davis, G. Luste, J. Martin, J. Prentice *et al.*, Phys. Rev. Lett. **43**, 1545 (1979).
[49] R. Egloff, P. Davis, G. Luste, J. Martin, J. Prentice *et al.*, Phys. Rev. Lett. **43**, 657 (1979).
[50] P. Frabetti *et al.* (E687 Collaboration), Phys. Lett. B **316**, 197 (1993).
[51] J. Ballam, G. Chadwick, M. Menke, P. Seyboth, Y. Eisenberg *et al.*, Phys. Rev. D **5**, 15 (1972).
[52] D. Aston *et al.* (Bonn-CERN-Ecole Poly-Glasgow-Lancaster-Manchester-Orsay-Paris-Rutherford-Sheffield Collaboration), Nucl. Phys. **B209**, 56 (1982).
[53] M. Atkinson *et al.* (Omega Photon Collaboration, Bonn-CERN-Glasgow-Lancaster-Manchester-Paris-Rutherford-Sheffield Collaboration), Nucl. Phys. **B231**, 15 (1984).
[54] J. Grosse-Knetter, Ph.D. dissertation, Universität Hamburg, 1997; Report No. DESY-F35 D-97-02.
[55] G. Antchev *et al.* (TOTEM Collaboration), Europhys. Lett. **101**, 21002 (2013).
[56] J. Beringer *et al.* (PDG), Phys. Rev. D **86**, 010001 (2012), http://pdg.lbl.gov/2012/hadronic-xsections/.
[57] U. Amaldi and K. R. Schubert, Nucl. Phys. **B166**, 301 (1980); A. Breakstone *et al.* (AMES-BOLOGNA-CERN-DORTMUND-HEIDELBERG-WARSAW COLLABORATION), Nucl. Phys. **B248**, 253 (1984); M. Bozzo *et al.* (UA4 Collaboration), Phys. Lett. **147B**, 392 (1984); N. A. Amos *et al.* (E-710 Collaboration), Phys. Lett. B **243**, 158 (1990).
[58] F. Abe *et al.* (CDF Collaboration), Phys. Rev. D **50**, 5518 (1994).
[59] P. Landshoff, AIP Conf. Proc. **1105**, 236 (2009).
[60] A. Brandt (D0 Collaboration), in *Proceedings of DIS 2010: XVIII International Workshop on Deep-Inelastic Scattering and Related Subjects* (Convitto della Calza, Firenze, Italy, 2010); *Proc. Sci.* DIS2010 (2010) 059; D0 Collaboration, Report No. 6056-CONF; S. L. Bueltmann, I. Chiang, R. Chrien, A. Drees, R. Gill *et al.*, Phys. Lett. B **579**, 245 (2004); N. A. Amos *et al.* (E710 Collaboration), Nuovo Cimento Soc. Ital. Fis. **106A**, 123 (1993); Phys. Rev. Lett. **68**, 2433 (1992); C. Augier *et al.* (UA4/2 Collaboration), Phys. Lett. B **316**, 448 (1993); M. Bozzo *et al.* (UA4 Collaboration), Phys. Lett. **147B**, 385 (1984); U. Amaldi *et al.* (CERN-Pisa-Rome-Stony Brook Collaboration), Phys. Lett. **62B**, 460 (1976); G. Barbiellini, M. Bozzo, P. Darriulat, G. Diambrini Palazzi, G. De Zorzi *et al.*, Phys. Lett. **39B**, 663 (1972); N. A. Amos, M. Block, G. Bobbink, M. Botje, D. Favart *et al.*, Nucl. Phys. **B262**, 689 (1985).